UCLA
UCLA Previously Published Works

Title

Molecular Dynamics Simulations Guide Chimeragenesis and Engineered Control of Chemoselectivity in Diketopiperazine Dimerases.

Permalink

https://escholarship.org/uc/item/95f898zz

Journal

Angewandte Chemie, 62(20)

Authors

Shende, Vikram
Harris, Natalia
Sanders, Jacob
et al.

Publication Date

2023-05-08

DOI

10.1002/anie.202210254

Peer reviewed

eScholarship.org Powered by the California Digital Library
University of California

Author Manuscript

Author Manuscript

Author Manuscript

Author Manuscript

HHS Public Access

Author manuscript

Angew Chem Int Ed Engl. Author manuscript; available in PMC 2024 May 08.

Published in final edited form as:

Angew Chem Int Ed Engl. 2023 May 08; 62(20): e202210254. doi:10.1002/anie.202210254.

Molecular Dynamics Simulations Guide Chimeragenesis and Engineered Control of Chemoselectivity in Diketopiperazine Dimerases

Vikram V. Shende[a], **Natalia R. Harris**[a], **Jacob N. Sanders**[b], **Sean A. Newmister**[a], **Yogan Khatri**[a], **Mohammad Movassaghi**[c], **K. N. Houk**[b], **David H. Sherman**[a]

[a]Life Sciences Institute, University of Michigan, Ann Arbor, Michigan 48109, United States

[b]Department of Chemistry and Biochemistry, University of California Los Angeles, Los Angeles, California

[c]Department of Chemistry, Massachusetts Institute of Technology, Cambridge, Massachusetts 02139, United States

Abstract

In the biosynthesis of the tryptophan-linked dimeric diketopiperazines (DKPs), cytochromes P450 selectively couple DKP monomers to generate a variety of intricate and isomeric frameworks. To determine the molecular basis for selectivity of these biocatalysts we obtained a high-resolution crystal structure of selective Csp^2–N bond forming dimerase, AspB. Overlay of the AspB structure onto C–C and C–N bond forming homolog NzeB revealed no significant structural variance to explain their divergent chemoselectivities. Molecular dynamics (MD) simulations identified a region of NzeB with increased conformational flexibility relative to AspB, and interchange of this region along with a single active site mutation led to a variant that catalyzes exclusive C–N bond formation. MD simulations also suggest that intermolecular C–C or C–N bond formation results from a change in mechanism, supported experimentally through use of a substrate mimic.

Graphical Abstract

davidhs@umich.edu; houk@chem.ucla.edu.
Institute and/or researcher Twitter usernames: K. N. Houk (@houk1000), David H. Sherman (@davidhsumich), Massachusetts Institute of Technology Department of Chemistry (@ChemistryMIT).

Conflict of Interest

The authors declare no conflict of interest.

Author Manuscript Author Manuscript Author Manuscript Author Manuscript

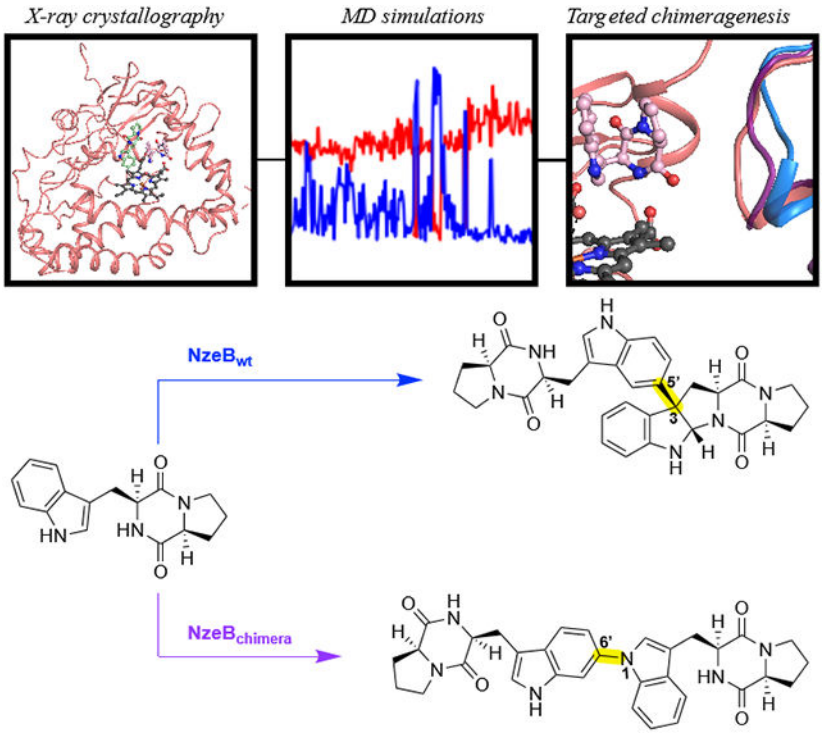

The high-resolution crystal structure of C–N bond forming diketopiperazine dimerase, AspB, was solved. However, the near complete superposition of active site residues and bound substrates in AspB/NzeB masked the molecular basis for their orthogonal chemoselectivities. Molecular dynamics simulations guided rational chimeragenesis to reprogram NzeB dimerase selectivity. Substrate mimics further validated differential substrate binding by the chemodivergent dimerases.

Keywords

natural products; biosynthesis; molecular dynamics; enzyme mechanisms; diketopiperazine

Diketopiperazine (DKP) natural products (NPs) have been isolated from all kingdoms of life, with over 1300 identified to date.[1] The structures of DKP-containing NPs are highly diverse, and many possess densely functionalized scaffolds as a result of extensive and selective enzymatic tailoring such as hydroxylation,[2,3] alkylation,[4] thiolation,[5] nitration,[6] nitrone oxidation,[7] desaturation,[8] dealkylation,[9] prenyltransfer and terpene cyclization,[10] oxidative cyclization,[11] coupling to nucleotides,[12] spirocyclization,[13,14] Diel-Alder cycloaddition,[15] and dimerization.[16] The tryptophan-linked dimeric DKP NPs are of particular interest as dimers are isolated both as single compounds and mixtures of constitutional isomers. This suggests that the selectivity of dimerization (and therefore site of C–H functionalization) is under enzymatic control.[17,18] Prior to the isolation of the (+)-naseseazine B (**1**), all tryptophan-linked DKP dimers had been isolated from fungi. Identification of new bacterial DKP dimers has expanded significantly in the past decade, including annotation of the associated biosynthetic gene clusters (BGCs) for (+)-naseseazine constitutional isomers (−)-naseseazine C (**2**)[19] and C–N bond-linked

Author Manuscript Author Manuscript Author Manuscript Author Manuscript

metabolite (−)-aspergilazine A (**3**).[20] Recently, bacterial dimers possessing connectivities previously observed exclusively from fungi such as tetratryptomycins A-C (**4**-**6**),[21] have been characterized, and the decoding of their BGCs provided access to soluble surrogates for fungal cytochromes P450 (P450s), including “fungal specific” scaffolds such as the $C_{7'}$-C_3-linked (+)-pestalazine A (**7**),[17,22] and $C_{7'}$-C_2-linked luchunazine D (**8**).[23]

Previously, we characterized the versatile DKP dimerase, NzeB, that catalyzes dimerization of brevianamide F (**9**) into carbon-carbon ($C_{6'}$–C_3) linked dimer, (+)-naseseazine B (**1**),[24,25] $C_{5'}$-C_3 linked (−)-naseseazine C (**2**)[26] as well as the carbon-nitrogen (C–N) linked dimer (−)-aspergilazine A (**3**).[27] Structural characterization of NzeB revealed two monomers of **9** bound in discrete pockets in the active site, and through mutagenesis of these residues we were able to abrogate formation of C–N linked dimers as well as perturb the product distribution of C–C linked dimers. However, neither homologous substitution nor alanine scanning mutagenesis of the NzeB active site generated a variant able to catalyze exclusive formation of the $C_{6'}$–N_1 linked dimer, **3**. Despite extensive screening, we were unable to capture NzeB-substrate complexes that displayed a binding mode with substrates preorganized to form the $C_{6'}$–N_1 dimerization axis found in **3**. Concomitant to our efforts, Yu et. al. identified dimerase AspB (97% amino acid identity to NzeB),[20] which exclusively catalyzes dimerization of **9** into **3**. Based on this new functional information, we hypothesized that the molecular basis for selective intermolecular $C_{6'}$–N_1 bond formation would become evident through structural characterization of P450 AspB.

To this end, we solved its x-ray crystal structure in complex with two units of **9** bound in the active site (PDB: 7S3J).[28] Despite their orthogonal chemoselectivity, the overall structure of AspB is completely superimposable with NzeB (root mean square deviation, RMSD=0.39 Å) and substrates in each enzyme are bound in coincident positions and conformations (Figure 2A). Despite this conservation of protein structure and substrate organization, we reasoned the single amino acid variation between active sites of AspB and NzeB (AspB = Ile68, NzeB = Gln68) may account for the observed switch in chemoselectivity and AspB’s ability to catalyze exclusive intermolecular $C_{6'}$–N_1 bond formation (Figure 2B). To evaluate the role of this active site variation in dimerization selectivity, we generated variant $NzeB_{Q68I}$. Dimerization reactions with $NzeB_{Q68I}$ resulted in increased production of **3**, however full reconstitution of AspB selectivity was not observed (Figure 2B). To identify potential substrate-enzyme interactions unique to AspB that may facilitate selective intermolecular $C_{6'}$–N_1 bond formation, we performed extensive alanine-scanning mutagenesis of the AspB active site and evaluated selectivity of these variants (Supporting Information, Supplementary Figure S3), however the resulting variants did not perturb the distribution of C–C or C–N linked dimers, implicating residues distal to the active site as drivers of dimerization chemoselectivity.

As the divergent selectivities of the NzeB/AspB dyad cannot be attributed to major variations in either sequence or structure, this motivated us to employ molecular dynamics (MD) simulations to identify the structural elements that influence dimerase selectivity.[29-31] Thus, we performed 1.2 microsecond simulations of each substrate-bound enzyme and, to identify regions with differential conformational plasticity, we computed the RMSD for the α-carbon of each residue (averaged over all three MD simulations) compared to the

Author Manuscript Author Manuscript Author Manuscript Author Manuscript

crystal structure (Figure 3). Comparing the α-carbon RMSD vs. residue number for NzeB and AspB revealed a region that appeared to be considerably less flexible in AspB from residues 86-91 (Figure 3a), which also corresponds to a region with low shared sequence homology (Supporting Information, Supplementary Figure S1). Overlays of representative snapshots of the protein backbone for residues 87-90 across all three MD simulations of both enzymes revealed that the higher RMSD for this region in NzeB (and absent in AspB) is explained by the presence of an additional cluster of conformations in which residues 87-90 move away from the active site (Figure 3B). Thus, we hypothesized the decrease in flexibility between residues 87-90 in AspB may be responsible for its ability to catalyze exclusively $C_{6'}$–N_1 bond formation. To functionally examine the role residues 87-90 play in the chemoselectivity of these enzymes, we generated a chimera of AspB and NzeB, using NzeB as a template, and the dimerization selectivity of the $NzeB_{G87A\text{-}A89G\text{-}I90V}$ was evaluated *in vitro* (Figure 4).

Analysis of the dimerization products of $NzeB_{G87A\text{-}A89G\text{-}I90V}$ revealed a significant shift in product distribution with a clear preference for $C_{6'}$–N_1 bond formation, albeit with diminished dimerization activity. Additionally, we generated and evaluated a series of chimeras from regions that MD simulations indicated were unlikely to affect selectivity, and indeed no significant change in product distribution was observed compared to wild-type NzeB (Figure 4B) and minimal perturbation of substrate turnover. We then incorporated the active site variation at residue 68 into the $NzeB_{G87A\text{-}A89G\text{-}I90V}$ chimera to generate $NzeB_{Q68I\text{-}G87A\text{-}A89G\text{-}I90V}$ and dimerization reactions with this new variant resulted in exclusive $C_{6'}$–N_1 bond formation. Structural characterization of the $NzeB_{Q68I\text{-}G87A\text{-}A89G\text{-}I90V}$ (PDB: 7S3T)[32] revealed a clear shift in the conformation of the chimeric region compared to wild-type NzeB (Figure 4A).

Previous quantum mechanical (QM) calculations, and high-resolution structures of NzeB, informed our mechanistic hypothesis that intermolecular C–C and C–N bond formation occurs via two distinct mechanisms.[27] Our QM calculations[27] posited that dimerization cascades leading to intermolecular C–C bond formation are initiated by abstraction of the DKP N_α–H by the P450 iron-oxo species (Figure 5A, atoms and arrows colored blue). Alternatively, dimerization reactions that result in formation of $C_{6'}$–N_1 bond linked dimers are initiated by indole N_1–H abstraction (Figure 5A, atom and arrows colored red). While N_1-indolyl radical and the pentacyclic C_3-carbon centered radical may interconvert, it is expected that their trapping by the dimerization partner in the active site may favor the formation of the respective products as illustrated. Comparative MD simulations of AspB and NzeB to identify the selectivity influencing regions also enabled examination of the variations in position and orientation of substrates bound in the active site of these two enzymes. MD simulations revealed that AspB maintains the indole N_1–H proximal to the iron-oxo throughout the trajectory (Figure 5B). By contrast, NzeB rapidly repositions the DKP N_α–H proximal to the P450 iron-oxo (Figure 5C), followed often by indole N_1–H and DKP N_α–H interchanging localization to the iron-oxo throughout the simulations (Supporting Information, Supplementary Figure S2), consistent with NzeB's ability to form both C–C and C–N bond linked dimers.

Author Manuscript Author Manuscript Author Manuscript Author Manuscript

These MD-simulations reinforce our mechanistic hypothesis that selectivity in dimerization is dependent on remodeling of the active site and repositioning of substrates upon formation of the reactive iron-oxo species. Given the innate challenge in generation, spectroscopic observation, and definitive assignment of substrate radical intermediates, we sought to focus on experimentally validating differential binding of substrates between C–C and C–N bond forming dimerases. Thus, we synthesized three substrate mimics incapable of N–H abstraction at the N_1–H and subjected them to dimerization conditions with AspB and NzeB. While reactions with probes **S1** and **S2** failed to show differential reactivity across all P450s examined, (Supporting Information, Supplementary Figures S18-S23), reactions with substrate **10** resulted in the generation of significant quantities of a new product exclusively formed by C–C bond forming P450 NzeB, and no observable products were formed in reactions with AspB (Figure 6). High-resolution mass spectrometry revealed a product with a m/z of 317.0952 ($M+H^+$) (calculated = 317.0954) indicative of a single oxygen insertion. Tandem MS/MS and NMR analysis enabled structural assignment of a new product **11** (Figure 6), which was further confirmed via chemical synthesis[33] and comparative analysis by HPLC (Figure 6, trace iv) and NMR. The selective formation of **11** by C–C bond forming dimerases and absence of reaction of **10** by C–N bond forming dimerases represents the first experimental evidence that chemodivergent dimerases position substrates differentially during catalysis despite completely superimposable x-ray structures.

In the current study, we determined the crystal structure of AspB, and while directed evolution campaigns have generated enzymes capable of catalyzing intra-[34] and intermolecular[35] C–H amination, AspB is the first structure of a wild-type cytochrome P450 that selectively catalyzes direct, intermolecular Csp^2–H amination. In an effort to distinguish the structural characteristics between AspB and chemodivergent homologue NzeB, we used MD simulations to compare overall conformational flexibility of these enzymes to uncover non-active site regions of the protein that control regioselectivity in DKP dimerization. Notably, models of AspB generated via AlphaFold[36] are also nearly superimposable with our experimentally determined structures of NzeB and AspB with no reorganization of active site architecture (Supporting Information, Supplementary Figure S29). These MD simulations guided our chimeragenesis, and through exchange of a non-active site region along with a single active site residue, we generated an NzeB chimera that fully reconstituted the selective C–N bond formation of wild-type AspB. In the course of our work, another group was able to achieve a similar goal through stochastic substitution of amino acid residues in DKP dimerases.[37] However, obtaining high-resolution crystal structures of the biochemically distinct homologues NzeB and AspB offered an opportunity to develop an alternative methodology for rational protein engineering: MD-guided targeted chimeragenesis. MD simulations also allowed us to visualize substrate position and repositioning in the active site of both enzymes in the presence of the P450 iron-oxo species, which reinforced our previous mechanistic hypothesis that dimerase chemoselectivity is dictated by substrate reorganization and selective N–H abstraction. Our results with substrate mimic **10** provide the first experimental evidence for differential substrate repositioning in C–C bond forming dimerases (NzeB/NascB) generating sulfoxide **11** compared to a lack of reactivity in the C–N bond forming dimerase (AspB). While MD simulations have guided rational engineering of enzymes,

Author Manuscript Author Manuscript Author Manuscript Author Manuscript

[29,38,39] this work demonstrates its predictive power and utility for visualizing alternate modes of substrate binding, conformational dynamics, and selectivity when confronted with nearly complete structural homology. We expect the demonstrated ability of "MD-targeted chimeragenesis" to identify selectivity motifs and guide protein engineering will be applicable beyond cytochromes P450 and can be employed to engineer a diverse range of chimeric enzymes with improved catalytic activity and non-native selectivities.

Supplementary Material

Refer to Web version on PubMed Central for supplementary material.

Acknowledgements

The authors acknowledge Dr. Osama G. Mohamed and Dr. Samantha P. Kelly for their guidance during isolation and structural characterization of oxidized products by NMR and MS/MS. We are grateful for support from the NSF CCI Center for Selective C–H Functionalization (CHE-1700982), NIH grant R35 GM118101, and the Hans W. Vahlteich Professorship (to D.H.S.). K.N.H. and M.M. acknowledge financial support from the NIH GM124480 and GM141963, respectively. J. N. S. acknowledges support from NIH F32 GM122218. Microsecond molecular dynamics simulations were performed using Anton 2 computer time provided by the Pittsburgh Supercomputing Center (PSC) through NIH GM116961. The Anton 2 machine at PSC was generously made available by D.E. Shaw Research. Additional computational resources were provided by the UCLA Institute for Digital Research and Education (IDRE).

Data availability statement

The data that support the findings of this study are available in the supplementary material of this article. Coordinates and structures have been deposited in the Protein Data Bank (PDB) under accession codes 7S3J and 7S3T.

References

[1]. Borthwick AD, Chem. Rev 2012, 112, 3641–3716. [PubMed: 22575049]

[2]. Patteson JB, Cai W, Johnson RA, Santa Maria KC, Li B, Biochemistry 2018, 57, 61–65. [PubMed: 29053243]

[3]. Meng S, Han W, Zhao J, Jian X, Pan H, Tang G, Angew. Chem. Int. Ed 2018, 57, 719–723.

[4]. Giessen TW, von Tesmar AM, Marahiel MA, Biochemistry 2013, 52, 4274–4283. [PubMed: 23705796]

[5]. Scharf DH, Remme N, Habel A, Chankhamjon P, Scherlach K, Heinekamp T, Hortschansky P, Brakhage AA, Hertweck C, J. Am. Chem. Soc 2011, 133, 12322–12325. [PubMed: 21749092]

[6]. Barry SM, Kers JA, Johnson EG, Song L, Aston PR, Patel B, Krasnoff SB, Crane BR, Gibson DM, Loria R, Challis GL, Nat Chem Biol 2012, 8, 814–816. [PubMed: 22941045]

[7]. Newmister SA, Gober CM, Romminger S, Yu F, Tripathi A, Parra LLL, Williams RM, Berlinck RGS, Joullié MM, Sherman DH, J. Am. Chem. Soc 2016, 138, 11176–11184. [PubMed: 27505044]

[8]. Lautru S, Gondry M, Genet R, Pernodet J-L, **n.d.**, 10.**n.d.**

[9]. Tsunematsu Y, Maeda N, Yokoyama M, Chankhamjon P, Watanabe K, Scherlach K, Hertweck C, Angew. Chem. Int. Ed 2018, 57, 14051–14054.

[10]. Yao T, Liu J, Liu Z, Li T, Li H, Che Q, Zhu T, Li D, Gu Q, Li W, Nat Commun 2018, 9, 4091. [PubMed: 30291234]

[11]. Lai C-Y, Lo I-W, Hewage RT, Chen Y-C, Chen C-T, Lee C-F, Lin S, Tang M-C, Lin H-C, Angew. Chem. Int. Ed 2017, 56, 9478–9482.

[12]. Liu J, Xie X, Li S, Angew. Chem. Int. Ed 2019, 58, 11534–11540.

Author Manuscript Author Manuscript Author Manuscript Author Manuscript

[13]. Li S, Finefield JM, Sunderhaus JD, McAfoos TJ, Williams RM, Sherman DH, J. Am. Chem. Soc 2012, 134, 788–791. [PubMed: 22188465]

[14]. Tsunematsu Y, Ishikawa N, Wakana D, Goda Y, Noguchi H, Moriya H, Hotta K, Watanabe K, Nat Chem Biol 2013, 9, 818–825. [PubMed: 24121553]

[15]. Ye Y, Du L, Zhang X, Newmister SA, McCauley M, Alegre-Requena JV, Zhang W, Mu S, Minami A, Fraley AE, Adrover-Castellano ML, Carney NA, Shende VV, Qi F, Oikawa H, Kato H, Tsukamoto S, Paton RS, Williams RM, Sherman DH, Li S, Nat Catal 2020, 3, 497–506. [PubMed: 32923978]

[16]. Saruwatari T, Yagishita F, Mino T, Noguchi H, Hotta K, Watanabe K, ChemBioChem 2014, 15, 656–659. [PubMed: 24677498]

[17]. Ding G, Jiang L, Guo L, Chen X, Zhang H, Che Y, J. Nat. Prod 2008, 71, 1861–1865. [PubMed: 18855443]

[18]. Li X-B, Li Y-L, Zhou J-C, Yuan H-Q, Wang X-N, Lou H-X, Journal of Asian Natural Products Research 2015, 17, 182–187. [PubMed: 25401948]

[19]. Tian W, Sun C, Zheng M, Harmer JR, Yu M, Zhang Y, Peng H, Zhu D, Deng Z, Chen S-L, Mobli M, Jia X, Qu X, Nat Commun 2018, 9, 4428. [PubMed: 30356123]

[20]. Yu H, Li S-M, Org. Lett 2019, 21, 7094–7098. [PubMed: 31429295]

[21]. Liu J, Xie X, Li S-M, Chem. Commun 2020, 56, 11042–11045.

[22]. Loach RP, Fenton OS, Movassaghi M, J. Am. Chem. Soc 2016, 138, 1057–1064. [PubMed: 26726924]

[23]. Sun S, Ma K, Tao Q, Han J, Bao L, Liu L, Liu H, Fitoterapia 2018, 125, 266–272. [PubMed: 29374569]

[24]. Raju R, Piggott AM, Conte M, Aalbersberg WGL, Feussner K, Capon RJ, Org. Lett 2009, 11, 3862–3865. [PubMed: 19655766]

[25]. Kim J, Movassaghi M, J. Am. Chem. Soc 2011, 133, 14940–14943. [PubMed: 21875056]

[26]. Buedenbender L, Grkovic T, Duffy S, Kurtböke DI, Avery VM, Carroll AR, Tetrahedron Letters 2016, 57, 5893–5895.

[27]. Shende VV, Khatri Y, Newmister SA, Sanders JN, Lindovska P, Yu F, Doyon TJ, Kim J, Houk KN, Movassaghi M, Sherman DH, J. Am. Chem. Soc 2020, 142, 17413–17424. [PubMed: 32786740]

[28]. Newmister SA, Shende VV, Harris NR, Sanders JN, Khatri Y, Movassaghi M, Houk KN, Sherman DH, Protein Data Bank 2021, DOI 10.2210/pdb7S3J/pdb.

[29]. Narayan ARH, Jiménez-Osés G, Liu P, Negretti S, Zhao W, Gilbert MM, Ramabhadran RO, Yang Y-F, Furan LR, Li Z, Podust LM, Montgomery J, Houk KN, Sherman DH, Nature Chem 2015, 7, 653–660. [PubMed: 26201742]

[30]. Gilbert MM, DeMars MD, Yang S, Grandner JM, Wang S, Wang H, Narayan ARH, Sherman DH, Houk KN, Montgomery J, ACS Cent. Sci 2017, 3, 1304–1310. [PubMed: 29296671]

[31]. DeMars MD, Samora NL, Yang S, Garcia-Borràs M, Sanders JN, Houk KN, Podust LM, Sherman DH, Journal of Biological Chemistry 2019, 294, 15947–15961. [PubMed: 31488542]

[32]. Harris NR, Shende VV, Sanders JN, Newmister SA, Khatri Y, Movassaghi M, Houk KN, Sherman DH, 2021, DOI 10.2210/pdb7S3T/pdb.

[33]. Sang R, Noble A, Aggarwal VK, Angew Chem Int Ed 2021, 60, 25313–25317.

[34]. McIntosh JA, Coelho PS, Farwell CC, Wang ZJ, Lewis JC, Brown TR, Arnold FH, Angew. Chem. Int. Ed 2013, 52, 9309–9312.

[35]. Prier CK, Zhang RK, Buller AR, Brinkmann-Chen S, Arnold FH, Nature Chem 2017, 9, 629–634. [PubMed: 28644476]

[36]. Mirdita M, Schütze K, Moriwaki Y, Heo L, Ovchinnikov S, Steinegger M, bioRxiv 2022, 2021.08.15.456425.

[37]. Sun C, Luo Z, Zhang W, Tian W, Peng H, Lin Z, Deng Z, Kobe B, Jia X, Qu X, Nat Commun 2020, 11, 6251. [PubMed: 33288748]

[38]. Yang S, DeMars MD, Grandner JM, Olson NM, Anzai Y, Sherman DH, Houk KN, J. Am. Chem. Soc 2020, 142, 17981–17988. [PubMed: 33030347]

Author Manuscript Author Manuscript Author Manuscript Author Manuscript

[39]. Dodani SC, Kiss G, Cahn JKB, Su Y, Pande VS, Arnold FH, Nature Chem 2016, 8, 419–425. [PubMed: 27102675]

Author Manuscript Author Manuscript Author Manuscript Author Manuscript

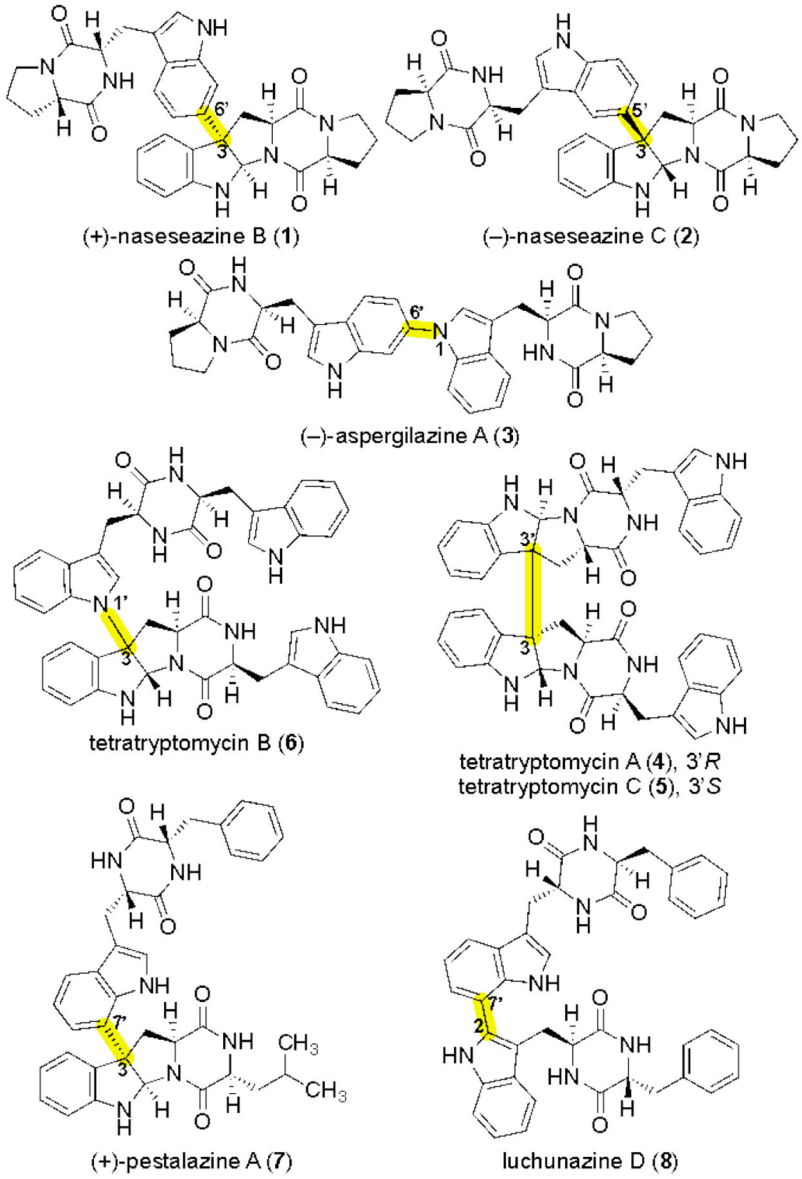

Figure 1.

Representative tryptophan-linked DKP homodimers representative of known dimerization connectivities found exclusively in bacteria (**1**-**2**), those common to bacteria and fungi (**3**-**6**), and exclusive to fungal DKP dimers (**7**-**8**).

Author Manuscript Author Manuscript Author Manuscript Author Manuscript

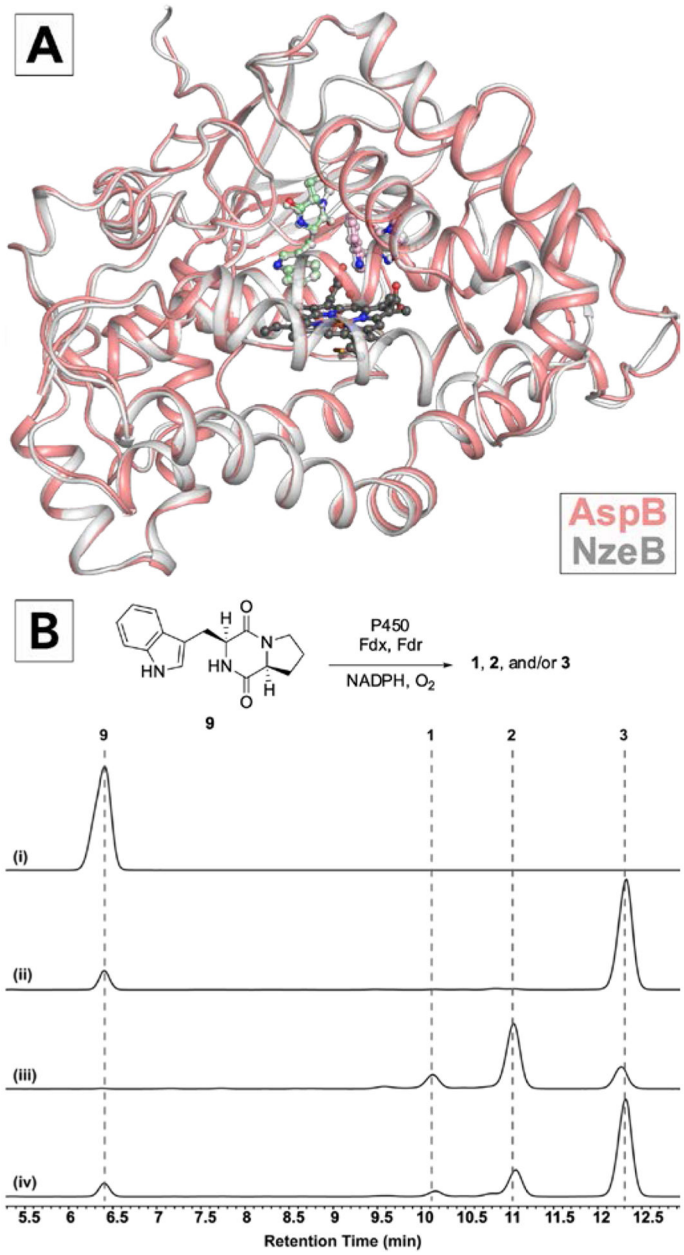

Figure 2.

A) Crystal structure of AspB (salmon) with substrates bound in cyclization site (pink) and dimerization site (mint green), heme (dark grey) and overlayed with NzeB (light grey) and its bound substrates (light grey). B) HPLC traces of (i) **9** synthetic standard, (ii) reaction of **9** with AspB, (iii) reaction of **9** with NzeB, and (iv) reaction of **9** with $NzeB_{Q68I}$. Fdx and Fdr are ferredoxin and ferredoxin reductase, respectively (*S. oleracea*).

Author Manuscript Author Manuscript Author Manuscript Author Manuscript

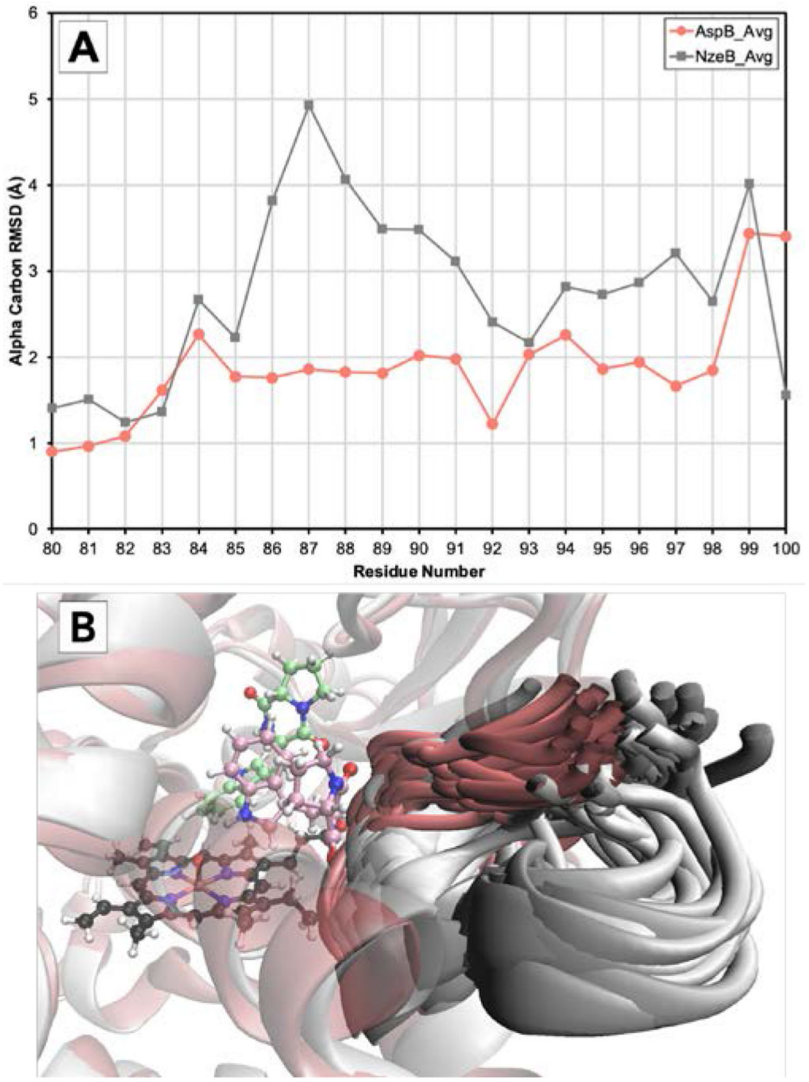

Figure 3.

A) RMSD for the α-carbon of amino acids 80-100 vs. residue number for NzeB (light grey) and AspB (salmon) averaged over three 1.2 microsecond MD simulations (NzeB heme in dark grey). B) Representative snapshots of the backbone of residues 87-90 for NzeB (light grey) and AspB (salmon) taken every 24 ns over all three 1.2 microsecond MD simulations.

Author Manuscript Author Manuscript Author Manuscript Author Manuscript

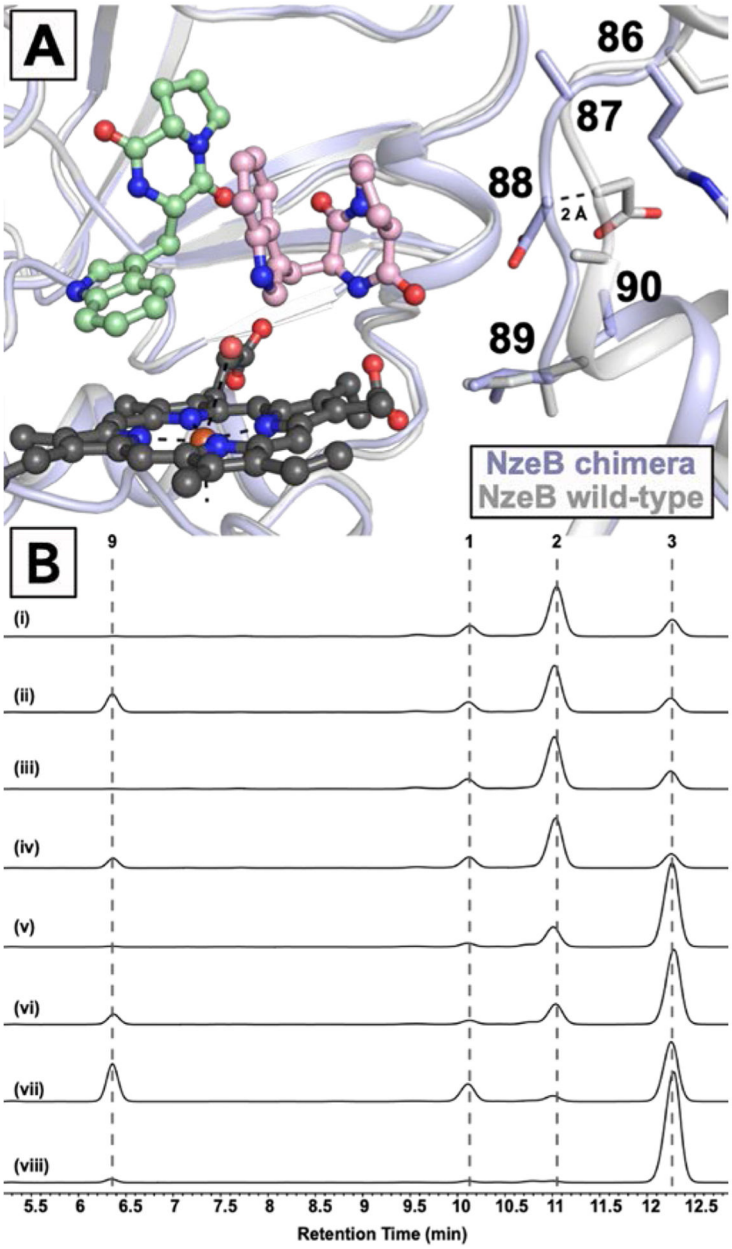

Figure 4.

A) Crystal structure of $NzeB_{Q68I\text{-}G87A\text{-}A89G\text{-}I90V}$ (light blue) and NzeB wt (grey) with chimeric region labeled. B) HPLC traces from reactions of **9** with (i) wild-type NzeB, (ii) $NzeB_{P43H\text{-}V47A}$, (iii) $NzeB_{T52A\text{-}K55E}$, (iv) $NzeB_{Q222H}$, (v) $NzeB_{S60P\text{-}F62L\text{-}Q68I}$, (vi) $NzeB_{Q68I}$, (vii) $NzeB_{G87A\text{-}A89G\text{-}I90V}$, (viii) $NzeB_{Q68I\text{-}G87A\text{-}A89G\text{-}I90V}$

Author Manuscript Author Manuscript Author Manuscript Author Manuscript

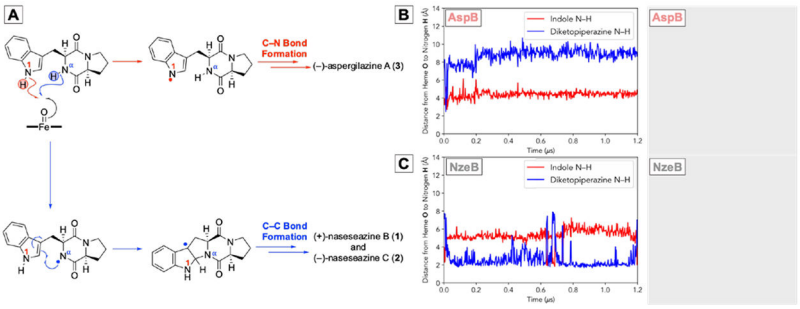

Figure 5.

A) Proposed mechanistic divergence between C–C and C–N bond formation catalyzed by DKP dimerases. B) Plot showing distance from P450 iron-oxo species to indole N_1–H (red) and DKP N_α–H (blue) over the course of a 1.2 microsecond MD simulation for AspB (left) and a representative snapshot for N_1–H abstraction catalyzed by AspB. C) Corresponding distance plot and representative snapshot for the N_α–H abstraction catalyzed by NzeB.

Author Manuscript Author Manuscript Author Manuscript Author Manuscript

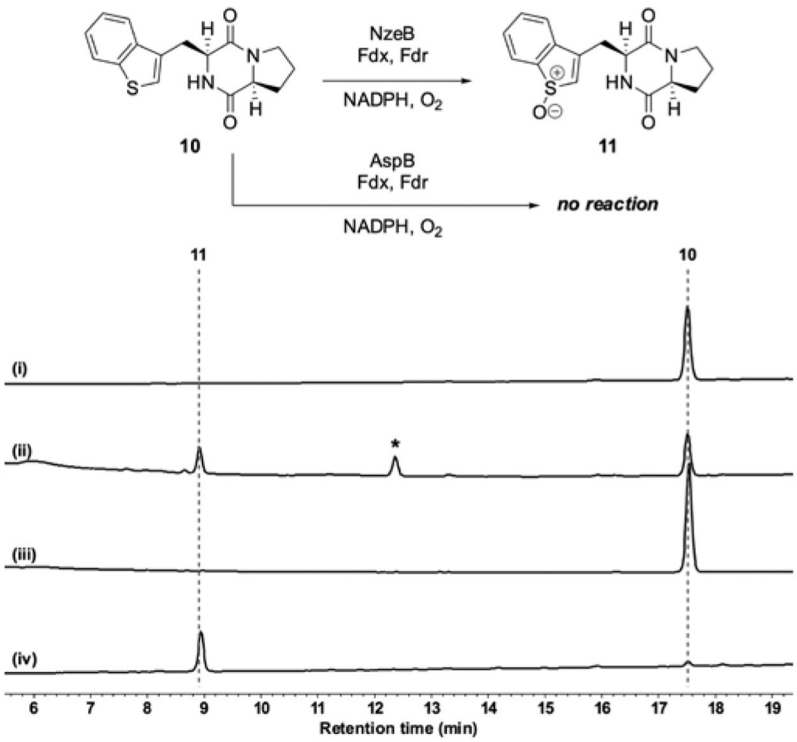

Figure 6.

HPLC traces for (i) synthetic standard of **10**, (ii) reactions of **10** with C–C bond forming dimerase NzeB and (iii) C–N bond forming dimerase AspB, and (iv) synthetic standard of **11**. Asterisk indicates benzothiophene sulfone which is also exclusively generated in reactions with C–C bond forming dimerases.